

AAEC/TM613



Library  
H.O.  
AAEC/TM613

**AUSTRALIAN ATOMIC ENERGY COMMISSION  
RESEARCH ESTABLISHMENT  
LUCAS HEIGHTS**

**APPLICATION OF THE PULSED NEUTRON TECHNIQUE  
TO FAST METAL SYSTEMS**

by

**S.P. MOO\*  
M.T. RAINBOW  
A.I.M. RITCHIE**

**\*University of Tasmania, Hobart**

**January 1973**

ISBN 642 99528 1



AUSTRALIAN ATOMIC ENERGY COMMISSION

RESEARCH ESTABLISHMENT

LUCAS HEIGHTS

APPLICATION OF THE PULSED NEUTRON TECHNIQUE

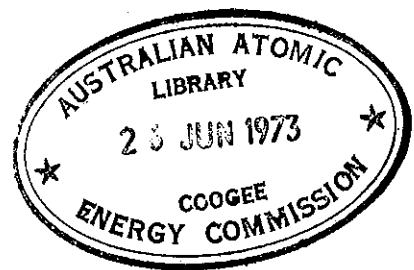
TO FAST METAL SYSTEMS

by

S. P. MOO\*

M. T. RAINBOW

A. I. M. RITCHIE



ABSTRACT

The experimental apparatus and techniques which have been developed up to the end of 1971 at the AAEC Research Establishment at Lucas Heights to allow pulsed experiments to be performed in fast metal systems are described. The details of a metallic thorium assembly, the pulsed neutron source, timing systems and shielding and room return problems are discussed.

---

\* University of Tasmania, Hobart.

National Library of Australia card number and ISBN 642 99528 1

The following descriptors have been selected from the INIS Thesaurus to describe the subject content of this report for information retrieval purposes. For further details please refer to IAEA-INIS-12 (INIS: Manual for Indexing) and IAEA-INIS-13 (INIS: Thesaurus) published in Vienna by the International Atomic Energy Agency.

BERYLLIUM; COUNTING RATES; ENERGY SPECTRA; FAST NEUTRONS;  
FISSION CHAMBERS; NEUTRON BEAMS; NEUTRON SOURCES; NEUTRON  
SPECTRA; NEUTRON TRANSPORT THEORY; NUCLEAR REACTION KINETICS;  
PREAMPLIFIERS; PULSED NEUTRON TECHNIQUES; RESOLUTION; SHIELDING;  
SLOWING-DOWN; TARGET; THORIUM; THRESHOLD DETECTORS; TIME DEPEND-  
ENCE; TIME-OF-FLIGHT METHOD

## CONTENTS

	<u>Page</u>
1. INTRODUCTION	1
2. THE FAST METAL ASSEMBLY	1
3. THE PULSED NEUTRON SOURCE	2
3.1 The Pulsed Source	2
3.2 Removal of d.c. Level and Higher Mass Components from the Pulsed Beam	3
4. TIMING SYSTEMS	4
4.1 Generation of Reference Timing Signals	5
4.2 Detectors	6
4.3 Generation of Detector Timing Signals	6
4.4 Time Measurements	6
4.5 Multidetector Measurements	7
5. TIMING ACCURACY AND STABILITY	8
5.1 Reference Timing Uncertainty	8
5.2 Detector Timing Uncertainty	9
5.3 Timing Stability	10
6. SHIELDING AND ROOM RETURN	10
7. SOME TYPICAL EXPERIMENTAL DATA	12
8. CONCLUSIONS	12
9. ACKNOWLEDGEMENTS	13
10. REFERENCES	13

Table 1 Impurity Specification for Thorium Metal

Figure 1 Schematic diagram of the thorium assembly and some associated facilities.

Figure 2 Angle integrated neutron energy spectrum from the  ${}^9\text{Be}(d,n){}^{10}\text{B}$  thick target reaction.

Figure 3 General plan view of the experimental area.

Figure 4 Effect of post acceleration deflection on  ${}^{239}\text{Pu}$  detector response.

Figure 5 Schematic diagram of the reference timing system.

Figure 6a Schematic diagram of the cross-over detector timing system.

Figure 6b Schematic diagram of the fast current preamplifier - A.R.C. detector timing system.

CONTENTS (Cont'd.)

- Figure 6c Schematic diagram of the NE-102 plastic scintillator timing system.
- Figure 7 Schematic diagram of the multidetector system.
- Figure 8 Schematic diagram of the system used for reference timing uncertainty measurements.
- Figure 9 Results of reference timing uncertainty measurements.
- Figure 10a Beam pulse profile measured with the NE-102 plastic scintillator.
- Figure 10b Result of detector timing uncertainty measurement with the cross-over detector timing system.
- Figure 10c Result of detector timing uncertainty measurement with the fast current preamplifier - A.R.C. detector timing system.
- Figure 11 Effect on  $^{239}\text{Pu}$  detector response of a boron shield at the surface of the thorium assembly.
- Figure 12 Time dependent reaction rate of a  $^{237}\text{Np}$  detector in the pulsed thorium assembly.
- Figure 13 Time dependent reaction rate of a  $^{235}\text{U}$  detector in the pulsed thorium assembly.

## 1. INTRODUCTION

The pulsed neutron technique has in the past been a powerful tool to complement static measurements in the study of neutron transport in thermal assemblies. In such assemblies there is usually an asymptotic mode of decay in which the neutron energy spectrum does not change with time and it is possible to measure decay constants which are characteristic of individual assemblies. In fast non-multiplying assemblies this is not the case in general since neutrons in these assemblies are continuously slowing down and the associated neutron energy spectra change continuously with time. However, this can be used to advantage since at different times after the pulse measured reaction rates are associated with different energy spectra and hence, with neutrons taking part in different physical processes. This is particularly so in materials of high atomic number since then there is little dispersion of the neutron energy spectrum during slowing down.

Pulsed experiments in fast systems are however intrinsically more difficult than similar measurements in thermal systems. There are two basic reasons for this.

- (i) The decay rates of neutron populations in fast systems are very much faster than those in thermal systems. The relaxation times in thermal systems are typically in the range 100  $\mu$ s to 1 ms while the time constants associated with detector reaction rates which are of interest in fast systems vary from hundreds of nanoseconds down to ~5 ns. These very much faster decay rates impose severe restrictions on the timing resolution of the experimental equipment
- (ii) It is much harder to prevent neutrons which have left the system being scattered back into the system. In thermal systems this 'room return' can be reduced to a negligible level by surrounding the system with strong thermal neutron absorber. This is effective since during most times of interest the majority of neutrons leaking from the system are thermal. However, this approach does not work with fast neutrons since in most nuclear interactions they are more likely to be scattered than absorbed.

The Pulsed Neutron Group of Physics Division at AAEC, Lucas Heights has extended its activities to the study of time dependent neutron transport in fast metal systems. This report describes the experimental apparatus and techniques which have been developed up to the end of 1971 to allow such experiments to be carried out.

## 2. THE FAST METAL ASSEMBLY

The assembly which is presently in use is constructed of metallic thorium

blocks, the majority of which are cubes of ~50 mm side. Some of the blocks have been modified to allow a 25 mm diameter accelerator beam flight tube to pass through the assembly (see Figure 1). In addition there are a set of smaller blocks which may be used to construct 13 mm square scan holes into the assembly. The largest assembly possible is a cube of dimensions ~0.4 x 0.4 x 0.4 m<sup>3</sup>.

The blocks were fabricated at Lucas Heights from metal powder by cold pressing and sintering. The density of individual blocks varies over the range 11.15 g cm<sup>-3</sup> to 11.4 g cm<sup>-3</sup>. Each of the blocks is coated with cellulose acetate lacquer to a thickness in the range 0.013 mm to 0.025 mm. An impurity specification of the thorium is presented in Table 1.

The thorium assembly rests on a three legged table of adjustable height (see Figure 1). The table top is a mild steel grate, 11 mm thick (see inset of Figure 1). It was made in this form to minimise the amount of material in the vicinity of the assembly and thus reduce backscatter of neutrons whilst providing sufficiently rigid support for the thorium assembly (total mass ~720 kg).

### 3. THE PULSED NEUTRON SOURCE

#### 3.1 The Pulsed Source

The basis of the pulsed neutron source is the modified (Fraser, Ritchie and Whittlestone 1968) 3 MeV Van de Graaff positive ion accelerator which can produce either proton or deuteron beams. Recent modifications (Fraser and Ritchie 1972) to this machine have improved and extended the earlier modifications and have increased the range of beam pulse widths and repetition rates available. In particular, these modifications allow the production of the following pulsed waveforms:-

- (i) Nominally square pulses with rise and fall times of ~17 ns with widths increasing from a minimum of ~50 ns FWHM at any repetition rate. This is the stepped beam deflection (S.B.D.) mode of pulsing.
- (ii) Nominally triangular pulses with a FWHM of 10 - 30 ns (nanosecond mode) or a FWHM of 2 - 5 ns (bunched mode) with a pulse period which is some integral number of microseconds. The width of pulses in these modes of operation depends on both ion source condition and the type of beam particle.

The <sup>9</sup>Be(d,n)<sup>10</sup>B reaction has been used exclusively to date and provides a copious source of neutrons. The neutron energy spectrum is, however, very broad as can be seen from Figure 2 which presents an angle integrated neutron energy spectrum for the reaction at a deuteron energy of 2.8 MeV, derived from

the angular distributions measured by Inada, Kawachi and Hiramoto (1968). The mean neutron energy here is  $\sim 2.7$  MeV.

It is proposed to use the  ${}^7\text{Li}(p,n){}^7\text{Be}$  reaction in the near future. This reaction, whilst it is not as copious a source of neutrons as the  ${}^9\text{Be}(d,n){}^{10}\text{B}$  reaction, is a threshold reaction. For this reason it is possible to produce a range of quite different neutron source spectra by adjusting the target thickness and the proton energy (Marion and Fowler, 1960).

A schematic diagram of the target assembly is included in Figure 1. The target, which may be either air or water cooled, is mounted at the end of two 0.9 m long concentric stainless steel tubes, the outer of which is polished and slides in a Wilson vacuum seal. The targets which are presently being used are 16 mm diameter, 3.2 mm thick beryllium metal discs which are fixed to the copper backing of the target assembly by a screw over brass shroud. The effective target area is circular with diameter 12.5 mm. The sliding target assembly allows the target to be located at any position along the beam axis within the thorium assembly, and at a limited range of positions outside the geometrical boundary of the assembly. In addition, the target may be completely removed from the beam flight path to permit beam usage further along the flight tube.

### 3.2 Removal of d.c. Level and Higher Mass Components from the Pulsed Beam

The pulsed beam, as it emerges from the accelerator, has two undesirable features, a non-negligible d.c. component and higher mass components, which are removed by a post acceleration deflection system.

The d.c. component of the beam varies between  $\sim 0.01$  per cent and  $\sim 0.2$  per cent of the current in the pulse depending upon the age and condition of the ion source. It is a problem since, if allowed to reach the target, a steady background of neutrons is produced in the thorium assembly.

A new ion source can produce a beam consisting of up to  $\sim 90$  per cent monatomic particles, whereas after a few hundred hours of operation, the monatomic beam may be only  $\sim 60$  per cent with the remainder made up of higher mass molecular ions. For a beam with energy 2.8 MeV, the time separation at the exit from the accelerator between a monatomic ion and an ion with twice the atomic mass, is  $\sim 135$  ns for protons and  $\sim 195$  ns for deuterons. The corresponding time separations at the target, which is  $\sim 10.65$  m from the accelerator, are  $\sim 325$  ns for protons and  $\sim 460$  ns for deuterons. Hence if the higher mass ions are not prevented from reaching the target they will produce pulses of neutrons during the period that the decay of the neutron population produced from the

main pulse is being measured.

The post acceleration deflection system consists of a deflection chamber and a fast 2 kV pulsing unit. The deflection chamber is located ~2.25 m from the accelerator (see Figure 3) and contains a pair of parallel plates. The plates are 1.3 m long, 50 mm wide and are separated by 25 mm. The fast pulsing unit was designed and built by Instrumentation and Control Division at Lucas Heights to produce nominal 2 kV square pulses with fast rise and fall times (~150 ns). These pulses are synchronised with the accelerator pulsing and applied to one deflection plate. A bias voltage of ~300 V is applied to the other plate to produce zero volts between the plates during the 'pulse-ON' period. The nominal 2 kV bias between the deflection plates during the 'pulse-OFF' period deflects the d.c. component of the beam.

Under usual operating conditions the beam pulse width is less than the time separation of the mass components of the beam at the post acceleration deflection chamber (~180 ns for protons and ~250 ns for deuterons at 2.8 MeV). In this case the 2 kV bias during the 'pulse-OFF' period deflects the higher mass components of the beam as well as the d.c. component from the target. For longer pulse lengths however a simple system, which involves a combination of magnetic and electrostatic deflection to remove higher mass components from the beam, has been successfully operated.

Figure 4 presents the time dependent response of a  $^{239}\text{Pu}$  pulse fission chamber in the thorium assembly following the injection of a fast neutron pulse. Two sets of results are presented; one set was obtained with the post acceleration deflection unit operating, the other set was obtained without post acceleration deflection. The results demonstrate that the unit is quite effective in removing the higher mass components. They also show that the 'background' level at long times (~1.5  $\mu\text{s}$  after the pulse) is reduced by a factor of two. This is much less than the effect on the d.c. current level of the accelerator beam which was reduced by a factor of at least two hundred. The remaining 'background' is attributed to the presence of 'room return' neutrons.

#### 4. TIMING SYSTEMS

The measurement of time dependent reaction rates in a pulsed assembly consists of determining the time of occurrence of events in the neutron detector with respect to the injection of a neutron pulse into the assembly. This requires

- (i) the generation of a reference timing signal which is related to the time of injection of the neutron pulse,

- (ii) the generation of detector timing signals which are related to the time of occurrence of events in the neutron detector,
- (iii) the measurement of the time interval between the reference and the detector timing signals.

#### 4.1 Generation of Reference Timing Signals

Figure 5 presents a schematic diagram of the electronics used for the generation of reference timing signals. The basis of this system is a capacitive beam pick-off (Anderson 1966) which is located within the beam flight tube ~200 mm from the front face of the thorium assembly (see Figure 1). It is protected from direct beam bombardment by a water cooled aperture which is located some 120 mm from the pick-off. The pick-off tube is 29 mm long, has an internal diameter of 14 mm, and has earthed guard rings with an internal diameter of 14 mm located at each end. The capacitance of the unit is 9 pF.

A beam pulse passing through the pick-off tube generates a signal which is fed to an impedance transformer (high input impedance, 50  $\Omega$  output impedance) which matches the signal to the rest of the timing equipment. Because of the high input impedance the signal from the impedance transformer is a good representation of the beam pulse profile, limited by the rise time of the unit which is of the order of 10 ns. This signal can be displayed on an oscilloscope to allow the beam pulse profile to be monitored during an experiment.

To date two types of impedance transformer have been used. One is an emitter follower similar to that described by Anderson (1966) which has an input impedance of ~300 k $\Omega$ . The other is a MOSFET device which has an input impedance of ~20 M $\Omega$ . Both of these units operate satisfactorily, but are not fast enough to monitor the shape of nanosecond and bunched beam pulses adequately. Efforts are presently being made to obtain a device with an input impedance of 10 M $\Omega$  and a rise time of 1.5 ns.

For timing purposes, the signal from the impedance transformer is fed to an ORTEC type 454 timing filter amplifier and thence to two ORTEC type 417 fast discriminators.

In the case of nanosecond and bunched beam pulsing the timing filter amplifier is used purely as a fast amplifier-inverter. However, in the case of S.B.D. (stepped beam deflection) beam pulsing, the timing filter amplifier is also used to differentiate the signal from the pick-off. Pulse inversion or non-inversion, in this case, determines whether the reference timing signals are related to either the leading or trailing edge of the S.B.D. pulses. The length of S.B.D. pulses varies from pulse to pulse. The jitter is typically 3 - 4 ns, but can be as large as 15 - 20 ns if the photomultipliers

in the top terminal of the accelerator which are used in this mode have been allowed to deteriorate (Fraser and Ritchie 1972). We have chosen to use reference timing signals which are related to the trailing edge of S.B.D. pulses.

The electronics following the timing filter amplifier are used to generate reference timing signals from the negative output of the timing filter amplifier. The discrimination level of discriminator 1 (Figure 5) is set to trigger as low as practicable to minimise time jitter due to any changes in the rise time or amplitude of the beam pulse. To guard against spurious signals which may arise because of the low discrimination level of discriminator 1, a second discriminator is set to trigger at a high level (negative). The positive logic output of this discriminator is used to generate a 50 ns wide negative gating pulse via the AAEC type 291 discriminator and the SAIP limiter which is fed to an EG & G Cl02B/N fast coincidence unit to produce overlap coincidence with genuine timing pulses from discriminator 1.

#### 4.2 Detectors

Twentieth Century type FC4B pulse fission chambers have been used exclusively for the pulsed measurements. These detectors are cylindrical ionisation chambers with 4.9 mm cathode diameter, 1.6 mm anode diameter, and 25 mm active length. The gas filling is argon with 2 per cent nitrogen at a pressure of 0.52 MPa. The fissile loading is in the form of a thin film of metal oxide on the cathode.

#### 4.3 Generation of Detector Timing Signals

During the setting up of equipment for these experiments, several different detector timing systems have been investigated. Initially a cross-over timing system operating in conjunction with a charge sensitive preamplifier (Figure 6a) was employed, but the system which has proved to be most satisfactory to date involves the use of a fast current preamplifier in conjunction with amplitude and rise time compensation (A.R.C.) timing.

Figure 6b presents a block diagram of the fast current preamplifier - A.R.C. timing system. The preamplifier was manufactured by Instrumentation and Control Division at Lucas Heights to the design of Rush (1964). The preamplifier output is amplified, but not shaped, by an ORTEC type 454 amplifier before processing by an ORTEC type 453 constant fraction timing discriminator and the fast negative logic output signal of this discriminator is used as the detector timing signal.

#### 4.4 Time Measurements

The measurement of the time interval between reference and detector timing

signals is performed by an ORTEC type 437 time to pulse height converter (TAC). The output of this unit is analysed by a Nuclear Data type ND-160F dual 1024 channel analogue to digital converter (ADC) in conjunction with a PDP-7 computer.

Because of dead times in the TAC associated with the operation of the TAC START, the reference timing signals derived from the beam pulses normally operate the TAC STOP in our measurements. This means that we normally measure the time interval between a detector event and the subsequent beam pulse.

#### 4.5 Multidetector Measurements

The sensitivity of the pulse fission chambers to fast neutrons is very low and the count rate of a single detector is typically  $\sim 100$  counts  $\text{sec}^{-1}$ . The count rate capability of the measuring system is limited by the ADC which is busy for  $\sim 200$   $\mu\text{s}$  per event. Thus the system is capable of handling count rates considerably higher than the count rates of our detectors before severe dead time effects are encountered. To allow more efficient use of accelerator time a routing facility has been designed and constructed which enables measurements with up to four detectors to be performed simultaneously. Figure 7 presents a block diagram of the multidetector system. The negative detector timing pulses are fed through an EG & G type OR 102/N fast or-gate to the TAC. The positive logic pulses associated with the detector timing pulses from the ORTEC type 453 discriminators are fed to an ADC interface unit (router) and may also be scaled. The action of the router is to set a bit on the address register of the ADC appropriate to the particular detector which has recorded an event. The computer is programmed to store time data in separate regions, each of which corresponds to a particular detector. The system is set up such that in the unlikely event of two or more detectors recording events within  $\sim 5$   $\mu\text{s}$  of each other then two or more data regions will be specified as corresponding to the particular timing signal which managed to trigger the TAC. In such cases, the event is rejected, but the occurrence is recorded in a coincidence table.

Scaling the routing pulses enables the actual number of detector events to be recorded and a dead time correction factor to be computed for the time analysed data.

It should be pointed out at this juncture that the number of neutron pulses injected into the assembly during these measurements exceeds the number of detector events recorded by more than three orders of magnitude. If such were not the case, then the use of a TAC could be suspect.

## 5. TIMING ACCURACY AND STABILITY

There are several parameters which may be used to specify the timing uncertainty of any system. The one which is most commonly used is the full width at half maximum (FWHM) of the timing uncertainty distribution. This parameter may easily be determined and is quite useful. However, it is unsuitable if one wishes to analyse the timing uncertainty of a system in terms of the timing uncertainties of components of that system, unless the timing uncertainties associated with the individual components are distributed in the same manner. For the purposes of this report we shall define the timing uncertainty of any system as the standard deviation of the timing uncertainty distribution. Since this parameter is related simply to the variance of the distribution, simple additive laws apply when analysing the timing uncertainty of a system in terms of the timing uncertainties associated with components of that system. This is the case even when the timing uncertainties associated with the individual components are quite differently distributed.

### 5.1 Reference Timing Uncertainty

Figure 8 presents a block diagram of a system which was set up to yield a measure of the timing uncertainty of the reference timing system described earlier (see Figure 5). In this case, however, two output pulses from the EG & G fast coincidence unit (gate 1) were used. One output was taken directly to the TAC STOP input; the other was fed to another gate, gate 2. The purpose of gate 2 was to reduce the pulse rate to the TAC START input. The gating pulse was also generated from discriminator 2 and was such as to allow only one timing pulse through every 5 ms. The timing pulses from gate 2 passed through an EG & G type DB463 delay unit to the TAC START input. The purpose of the delay unit was to allow the START timing pulses to be conveniently delayed with respect to the STOP timing pulses. The TAC then measured the time interval between a timing pulse generated from a particular nanosecond beam pulse and the timing pulse generated from the subsequent beam pulse (apart from the fixed delays in the system).

Figure 9 presents a plot of results obtained from measurements with this system. The second and third peaks were obtained by decreasing the calibrated delay in the START line by 50 ns and 100 ns respectively. These results show that the channel width is  $1.243 \pm 0.015$  ns and the standard deviations of the distributions in the first, second and third peaks are  $\pm 0.85$  ns,  $\pm 0.86$  ns and  $\pm 0.88$  ns respectively.

It should be noted that each of these measured timing uncertainty distributions consists of a double contribution from the timing jitter associated

with the generation of timing signals and a single contribution from the jitter on the time interval between consecutive nanosecond beam pulses. Thus, the timing uncertainty of the reference timing system in the case of nanosecond beam pulsing is less than  $\pm 0.9$  ns. A similar examination of the reference timing uncertainty in the case of S.B.D. beam pulsing is yet to be made.

## 5.2 Detector Timing Uncertainty

An absolute determination of the timing uncertainties of the detector timing systems would be extremely difficult since it requires that the time of occurrence of fission events in the detector be known very accurately. However, upper and lower bounds on the timing uncertainties of the detector timing systems have been estimated by measuring the time response of the systems to narrow bursts of neutrons which define, to a limited extent, the time at which the fission events occur.

Neutron bursts were produced by the  ${}^9\text{Be}(d,n){}^{10}\text{B}$  reaction using klystron bunched beam pulses from the accelerator. An estimate of the neutron pulse profile at the beryllium target was obtained by time analysing the output of an NE-102 plastic scintillator which detected the gamma flash (associated with neutron production) from the target. The scintillator timing system is shown schematically in Figure 6c. The timing uncertainty of this system was not measured, but is probably  $\lesssim \pm 0.5$  ns.

Since the source produces neutrons with energies ranging from  $\sim 10$  keV up to  $\sim 8$  MeV, the neutron pulse is strongly dispersed in time as a function of distance from the source. To reduce these time of flight effects to a reasonable level, the detector was located as near as possible to ( $\sim 20$  mm from) the source. Moreover a  ${}^{237}\text{Np}$  pulse fission chamber was used exclusively in these measurements, since the 400 keV  ${}^{237}\text{Np}$  fission cross section threshold further restricts the important range of neutron energies to 400 keV - 8 MeV. The corresponding flight times over the 20 mm flight path are 2.3 ns and 0.5 ns respectively. The effect of scattered neutrons was minimised by having as little material as possible in the vicinity of the source.

Figure 10a presents the time dependent response of the plastic scintillator (NE-102). Figures 10b and 10c present the time analysed responses of the  ${}^{237}\text{Np}$  detector using the cross-over timing system and the fast current preamplifier - A.R.C. timing system respectively. The standard deviations of the measured time distributions in each case were  $\pm 3.8$  ns,  $\pm 15.8$  ns and  $\pm 5.1$  ns. Obviously the fast current preamplifier - A.R.C. timing system is far superior to the cross-over timing system in this application.

The timing uncertainty of the  ${}^{237}\text{Np}$  detector cross-over timing system and

fast current preamplifier - A.R.C. timing system respectively are in the ranges  $\pm 15.3$  to  $\pm 15.8$  ns and  $\pm 3.3$  to  $\pm 5.0$  ms. The upper limits were obtained by assuming:

- (i) the standard deviation of the distribution of neutron flight times is  $\pm 0.9$  ns,
- (ii) the neutron pulse is a  $\delta$ -function in time at the source, and
- (iii) the reference timing uncertainty is  $\pm 0.9$  ns.

The lower limits were obtained by assuming:

- (i) the standard deviation of the distribution of neutron flight times is  $\pm 0.9$  ns,
- (ii) that the scintillator system measures the neutron pulse profile at the target exactly, apart from the timing uncertainty associated with the reference timing system which is common to both the NE-102 and  $^{237}\text{Np}$  measurements.

Similar measurements with the non-threshold detectors are quite severely affected by neutron pulse dispersion over the 20 mm flight path and would be difficult to analyse. Since the non-threshold detectors differ from the  $^{237}\text{Np}$  detector only in the type of fissile loading, we assume that the timing properties of the timing systems incorporating a non-threshold detector will be similar to those measured for the timing systems incorporating the  $^{237}\text{Np}$  detector.

### 5.3 Timing Stability

Recent measurements of spatial distributions of both  $^{237}\text{Np}$  and  $^{235}\text{U}$  detector reaction rates have extended over periods of two to three days during which the total observed time drift was less than 0.5 ns. The chief cause of these long term time shifts appears to be changes in accelerator performance. The shape and amplitude of the beam pulse and the machine energy usually change slightly over an extended period and lead to shifts in the time relationship of the reference timing signals with respect to the neutron pulses.

## 6. SHIELDING AND ROOM RETURN

The nearest massive scattering medium to the thorium assembly and therefore probably the greatest source of room return neutrons, is the concrete floor of the experimental area which is only 1.06 m below the centre of the assembly. Unfortunately, because it has not been possible to move the assembly with respect to the floor, it has not been possible to satisfactorily examine room return associated with this source. However, in spite of this, a series of die-away measurements with non-threshold detectors, was performed to examine

- (i) the effect of borated paraffin floor and walls about the assembly (see Figures 1 and 3),
- (ii) the effect of the table which supports the assembly and
- (iii) the effect of cadmium, boral and boron carbide shields at the surface of the assembly.

The measurements to examine (i) and (ii) indicated that the time dependent reaction rate of a  $^{239}\text{Pu}$  detector in the thorium assembly was not affected by the 150 mm thick borated paraffin floor and walls and the supporting table to within the experimental accuracy attainable at the time of the measurements. However, the detector response was significantly affected by cadmium, boral and boron carbide shields at the surface of the assembly. Figure 11 presents time dependent  $^{239}\text{Pu}$  reaction rates and shows the effect of surrounding the assembly with 6 mm boral plate. The boral shield reduced the long term 'background' which must be mainly due to low energy neutrons. The results also show that the decay of the neutron population in the assembly with a boral shield is somewhat slower during the first 400 ns or so after the pulse, than the decay in the absence of a boral shield. As this effect was observed with each shield and did not differ very much from one position to another within the assembly it was attributed to backscatter from the shields.

Because it was not possible to examine room return effects associated with the floor, further study of the room return problem for measurements with non-threshold detectors was deferred until an elevated low scattering facility, which is due to be installed in the latter half of 1972, becomes available. In the meantime attention has been directed to measurements with threshold pulse fission chambers and with non-threshold fission detectors over the restricted time interval after the pulse ( $\sim 200$  ns) during which room scattered neutrons will not have had sufficient time to return to the assembly. This time interval is sufficiently long to place no significant limitations on measurements with the threshold fission detectors since the 'decay times' are very short ( $\sim 15$  ns for  $^{237}\text{Np}$  and  $\sim 5$  ns for  $^{238}\text{U}$ ) with the  $^9\text{Be}(d,n)^{10}\text{B}$  pulsed source.

The experimental arrangement which is used for these measurements consists of

- (i) the bare thorium assembly supported by the table described earlier,
- (ii) a 150 mm thick borated paraffin floor in the shape of a regular dodecagon of side 1.02 m (the diameter of the inscribed circle is  $\sim 3.8$  m), which is centred on the thorium assembly and covers the concrete floor of the experimental area,
- (iii) 150 mm thick borated paraffin walls which are mounted along the

perimeter of the borated paraffin floor to a height of 2.1 m above the concrete floor.

Apart from the supporting table, the scattering medium which is closest to the thorium assembly is the borated paraffin floor which is ~0.9 m below the centre of the assembly. Neutrons from the  ${}^9\text{Be}(d,n){}^{10}\text{B}$  reaction have energies in the range ~10 keV to ~8 MeV with mean energy ~2.7 MeV (for 2.8 MeV deuterons). An 8 MeV neutron, which travels at a speed of  $3.94 \text{ cm ns}^{-1}$ , would take at least 46 ns to travel from the source to the floor and back to the assembly without any significant loss of energy; a 2.5 MeV neutron would take at least 80 ns. Covering the floor with borated paraffin ensures that a large number of neutrons lose quite an amount of energy before the return flight to the thorium assembly and, as a consequence, have the time of their return flight extended considerably. In addition, for the case of threshold detectors, the room return neutrons are very likely to have energies below the threshold energies. It is worthy of note that longer 'room return free' measuring times would be available if the  ${}^7\text{Li}(p,n){}^7\text{Be}$  reaction were used as the neutron source because source neutron energies can be, and are in general, lower.

#### 7. SOME TYPICAL EXPERIMENTAL DATA

Figures 12 and 13 present plots of the time dependent reaction rates of  ${}^{237}\text{Np}$  and  ${}^{235}\text{U}$  detectors in the thorium assembly following the injection of a pulse of fast neutrons. Both sets of results were obtained with the accelerator operating in its nanosecond mode at 2.8 MeV with the  ${}^9\text{Be}(d,n){}^{10}\text{B}$  reaction being used as the neutron source.

Figure 12 demonstrates that the  ${}^{237}\text{Np}$  reaction rate decays very quickly, viz. through two decades of count rate in less than 100 ns. Figure 13 demonstrates that the time dependent reaction rate of  ${}^{235}\text{U}$  persists for far longer than that of  ${}^{237}\text{Np}$ . Room return is, as has already been indicated, a possible problem for the  ${}^{235}\text{U}$  response at 'late' times after the pulse. For this reason the time domain over which  ${}^{235}\text{U}$  data is analysed has been restricted.

#### 8. CONCLUSIONS

This report has described the experimental systems and techniques developed up to the end of 1971 to allow the study of neutron transport in metal systems by the pulsed neutron method. The timing resolution of better than  $\pm 5 \text{ ns}$  obtained with commercially available pulse fission chambers is well within the requirements for carrying out useful time dependent reaction rate measurements with detectors having a broad range energy response (e.g.  ${}^{239}\text{Pu}$ ,  ${}^{233}\text{U}$ ,  ${}^{235}\text{U}$ , etc.). The decay rate of threshold reactions with thresholds at a relatively low energy, such as  ${}^{237}\text{Np}$ , can also be measured successfully, but

with a source energy of  $\sim 2.7$  MeV the decay rate of those reactions with higher threshold energies, such as  $^{238}\text{U}$ , would be significantly affected by resolution broadening.

The importance of room return neutrons has not been satisfactorily evaluated. Until the installation of an elevated low scattering facility this problem has been circumvented by limiting investigations to the time period after the pulse during which neutrons have had insufficient time to leak from the assembly and then be scattered back into it. This has placed no significant limitations on measurements with  $^{237}\text{Np}$ .

The instantaneous decay constant of the fundamental Fourier spatial mode can be measured over the restricted time range with a precision better than 2 per cent for  $^{237}\text{Np}$ ,  $^{239}\text{Pu}$  and  $^{235}\text{U}$  when the  $^9\text{Be}(d,n)^{10}\text{B}$  reaction is used as the neutron source.

It is expected that further advances will be made in improving the timing resolution. The advent of the elevated low scattering facility will allow measurements with non-threshold detectors to be performed over a longer time range, and more work to be done to assess the effect of room return neutrons.

#### 9. ACKNOWLEDGEMENTS

We wish to express our gratitude to the technical staff of Physics Division at the AAEC Research Establishment for their assistance during the course of this development. One of us, S.P. Moo, wishes to acknowledge the Australian Institute of Nuclear Science and Engineering for its generous grant to the University of Tasmania in support of this work and to thank Drs. K.B. Fenton and A.G. Fenton of the University of Tasmania for their continued interest and support.

#### 10. REFERENCES

- Anderson, J.H. (1966) - AWRE O-53/66.
- Fraser, H.J., Ritchie, A.I.M. and Whittlestone, S. (1968) - Rev. Scient. Instrum., 39 : 240.
- Fraser, H.J. and Ritchie, A.I.M. (1972) - submitted to Nucl. Instrum. and Methods.
- Inada, T., Kawachi, K. and Hiramoto, T. (1968) - J. Nucl. Sci. and Technol., 5 : 22.
- Marion, J.B., and Fowler, J.L. (1960) - 'Fast Neutron Physics - Part I', Interscience Publishers Inc. (New York).
- Rush, C.J. (1964) - Rev. Scient. Instrum., 35 : 149.



TABLE 1

IMPURITY SPECIFICATION FOR THORIUM METAL

Element	Maximum Concentration ppm
Nitrogen	< 150
Oxygen	< 5,500
Hydrogen	< 500
Iron	< 200
Calcium	< 250
Aluminium	< 800
Silicon	< 100
Manganese	< 20
Chlorine	< 100



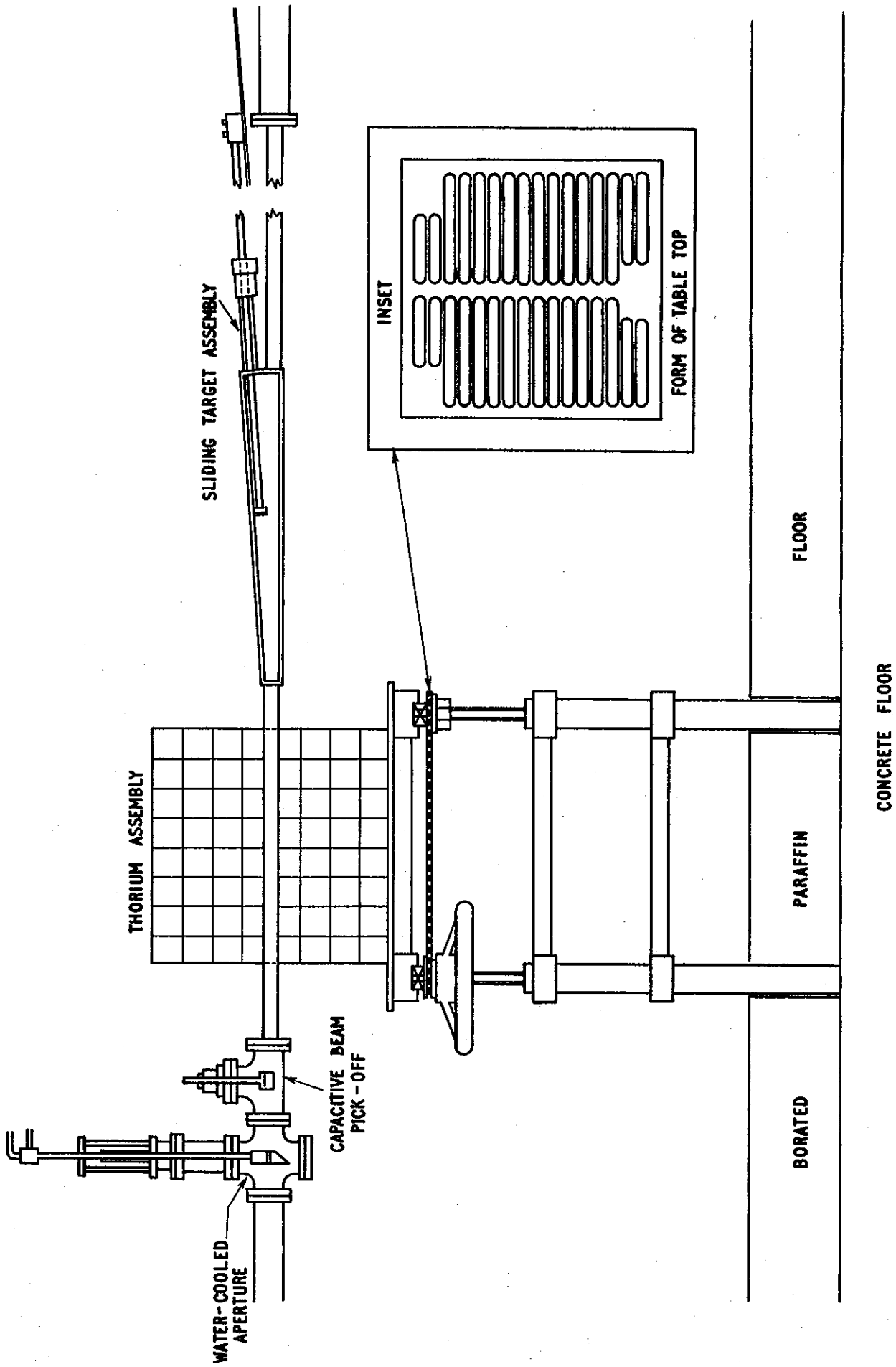


FIGURE 1. SCHEMATIC DIAGRAM OF THE THORIUM ASSEMBLY AND SOME ASSOCIATED FACILITIES

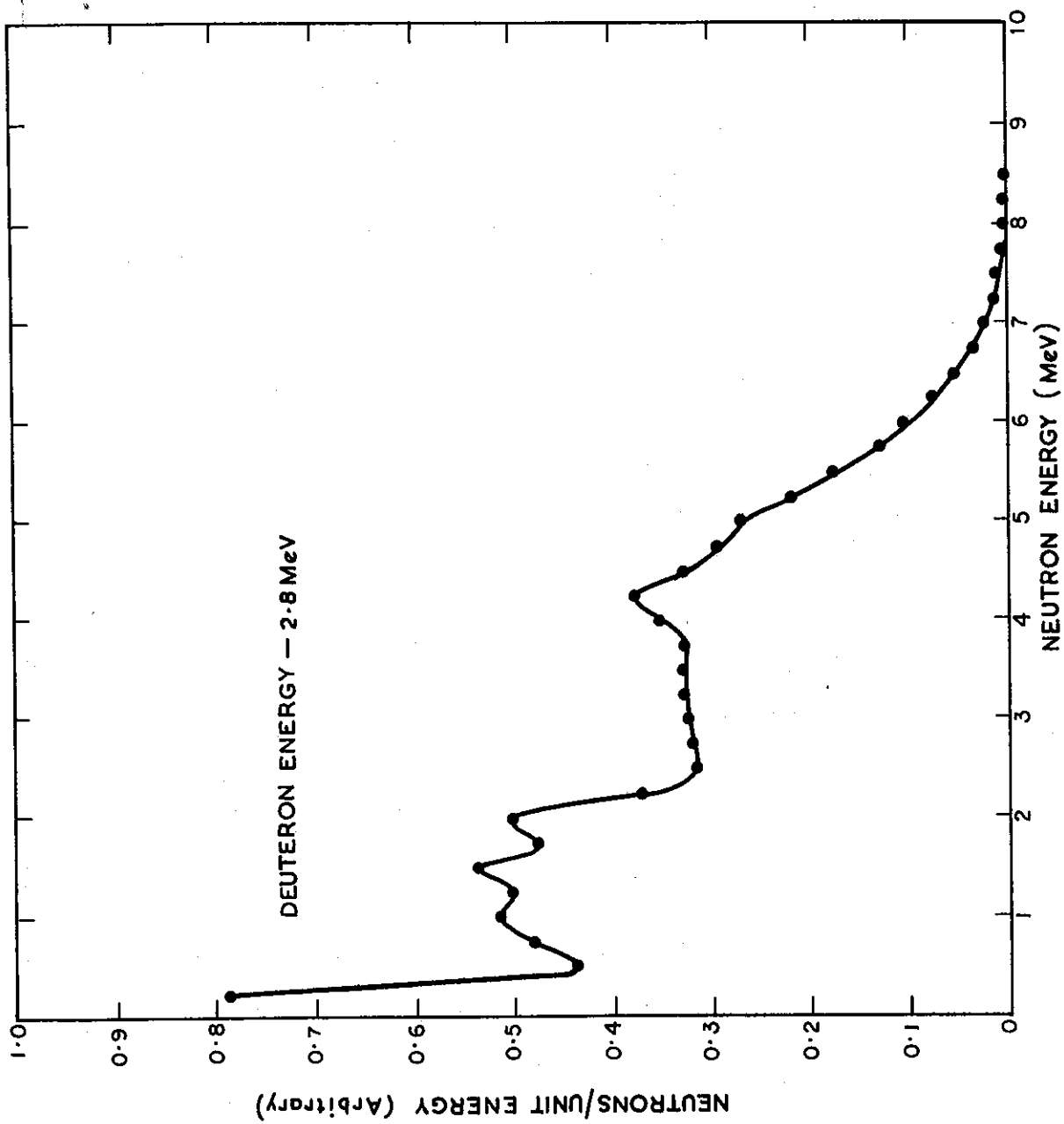


FIGURE 2. ANGLE INTEGRATED NEUTRON ENERGY SPECTRUM FROM THE  ${}^9\text{Be}(d,n){}^{10}\text{B}$  THICK TARGET REACTION

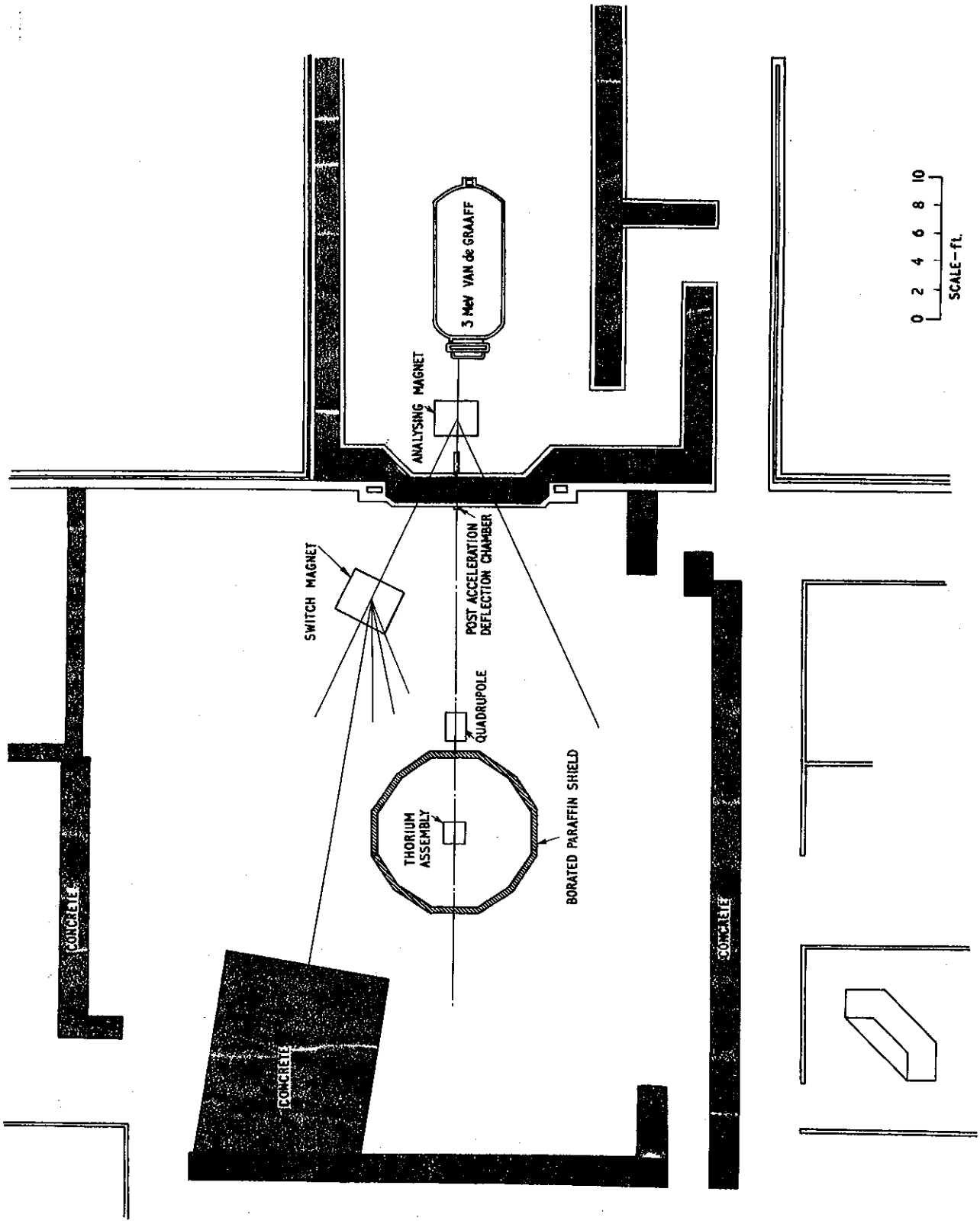


FIGURE 3. GENERAL PLAN VIEW OF THE EXPERIMENTAL AREA.

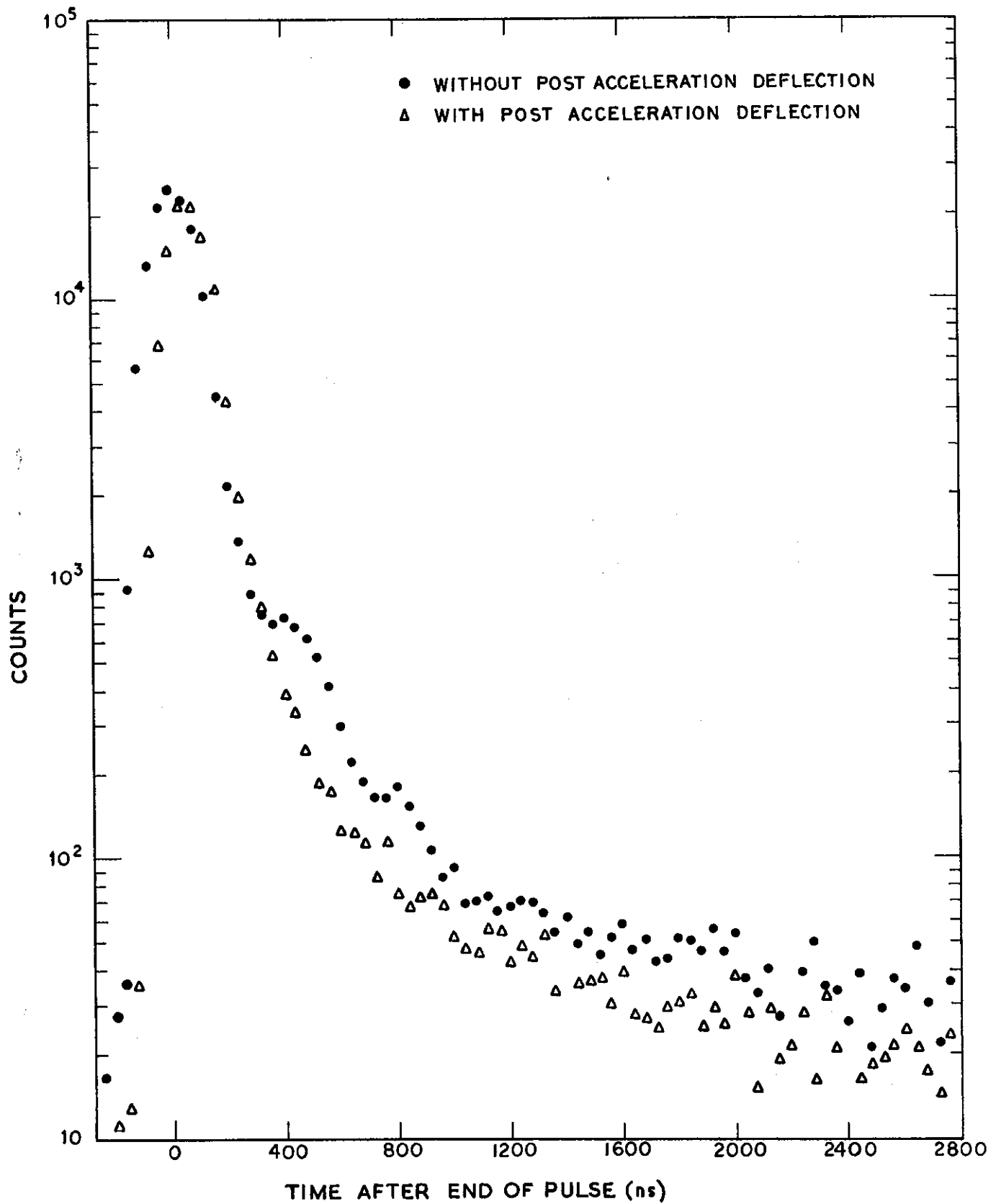


FIGURE 4. EFFECT OF POST ACCELERATION DEFLECTION ON  $^{239}\text{Pu}$  DETECTOR RESPONSE

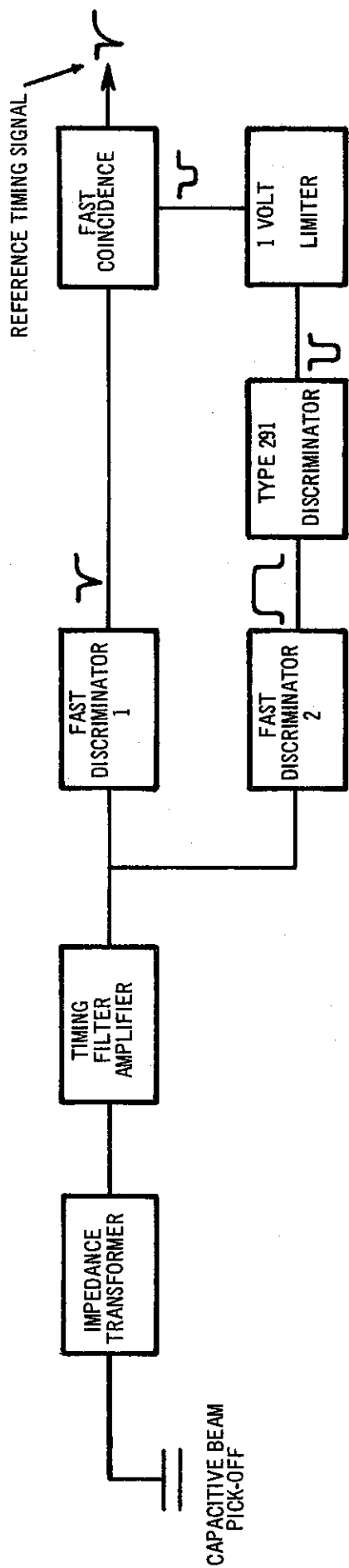


FIGURE 5. SCHEMATIC DIAGRAM OF THE REFERENCE TIMING SYSTEM

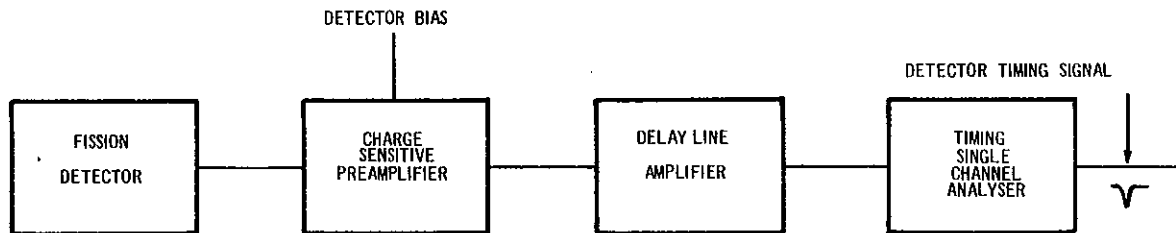


FIGURE 6a. SCHEMATIC DIAGRAM OF THE CROSS-OVER DETECTOR TIMING SYSTEM

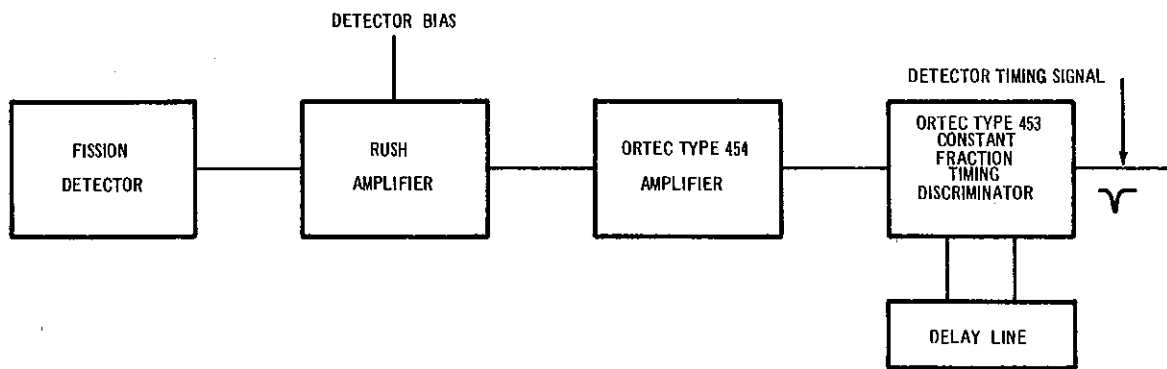


FIGURE 6b. SCHEMATIC DIAGRAM OF THE FAST CURRENT PREAMPLIFIER -  
A.R.C. DETECTOR TIMING SYSTEM

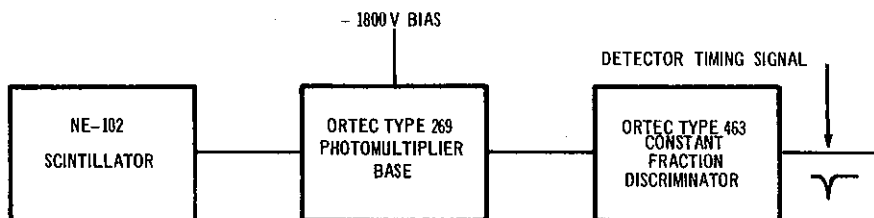
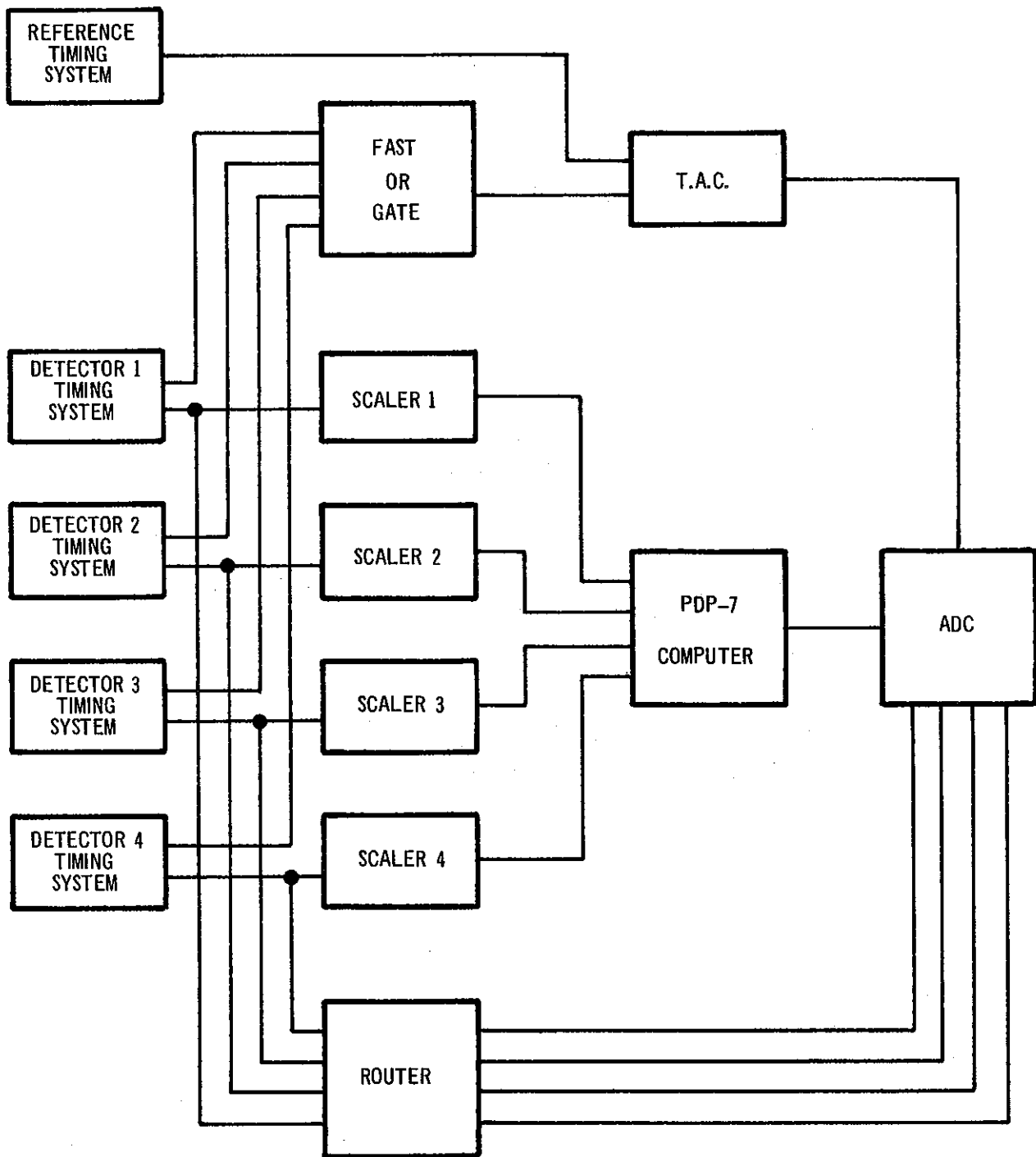
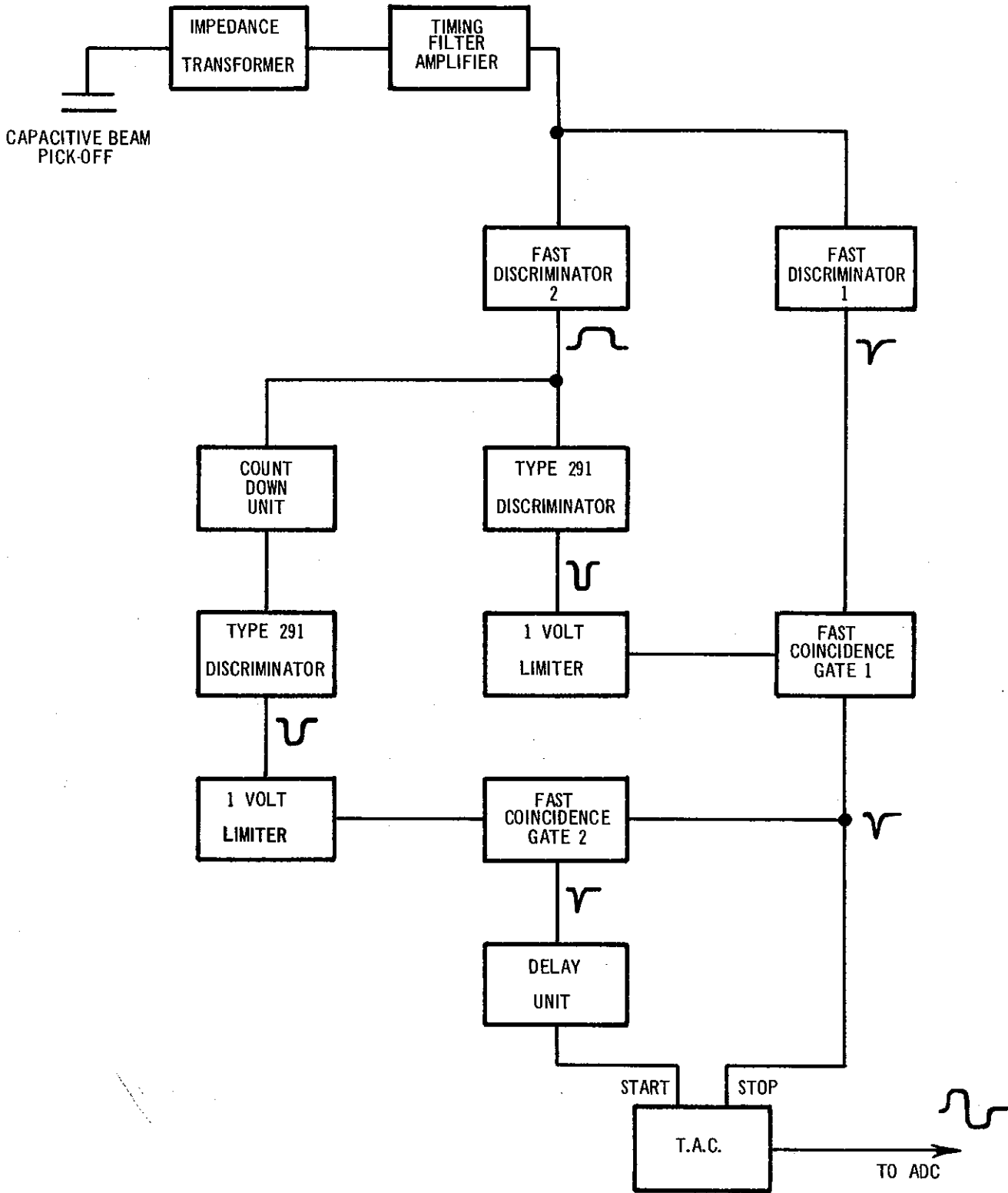


FIGURE 6c. SCHEMATIC DIAGRAM OF THE NE-102 PLASTIC SCINTILLATOR TIMING SYSTEM



**FIGURE 7. SCHEMATIC DIAGRAM OF THE MULTIDECTOR SYSTEM**



**FIGURE 8. SCHEMATIC DIAGRAM OF THE SYSTEM USED FOR REFERENCE TIMING UNCERTAINTY MEASUREMENTS**

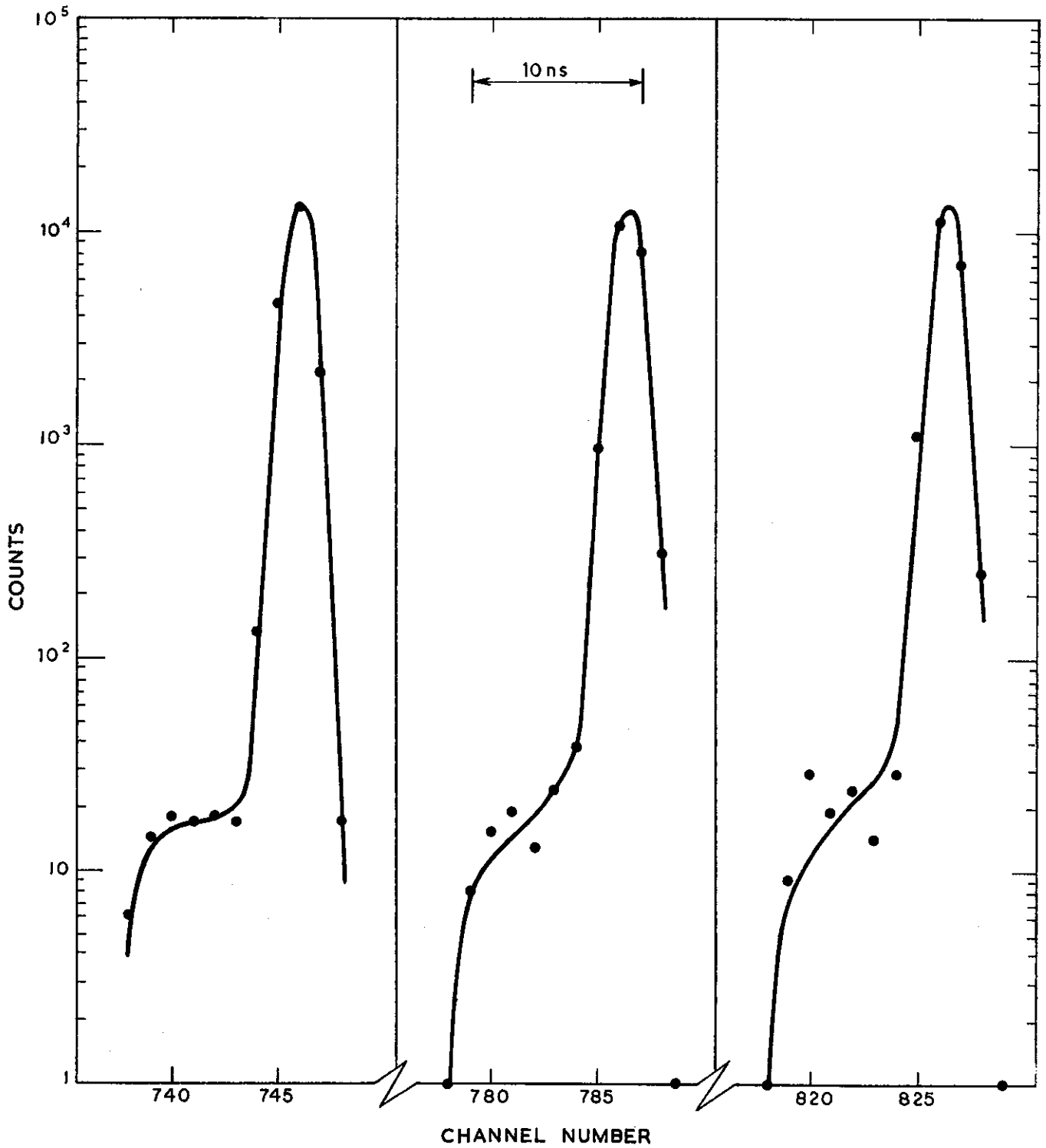


FIGURE 9. RESULTS OF REFERENCE TIMING UNCERTAINTY MEASUREMENTS

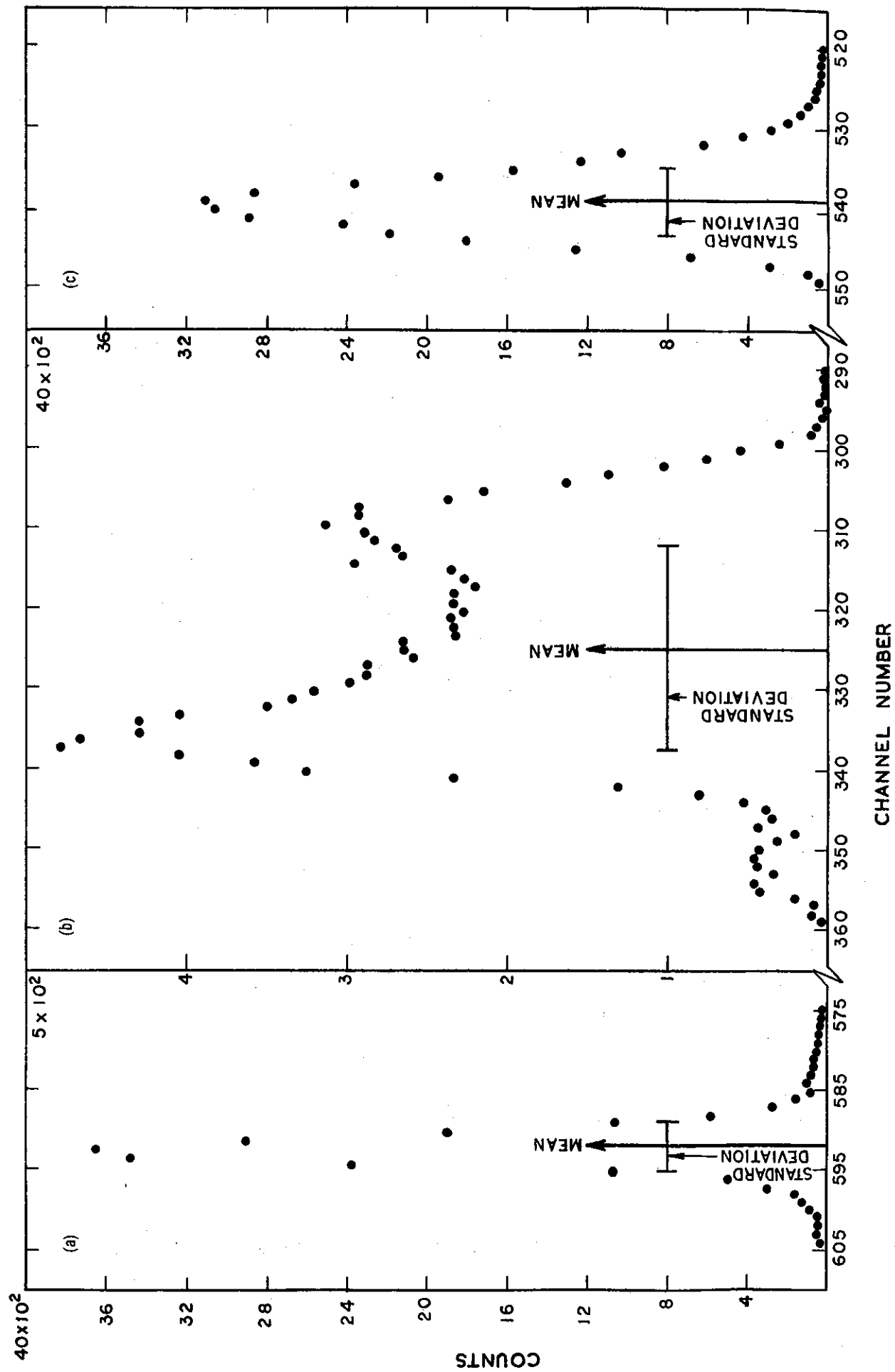


FIGURE 10 a BEAM PULSE PROFILE MEASURED WITH THE NE-102 PLASTIC SCINTILLATOR

FIGURE 10 b RESULT OF DETECTOR TIMING UNCERTAINTY MEASUREMENT WITH THE CROSS-OVER DETECTOR TIMING SYSTEM

FIGURE 10 c RESULT OF DETECTOR TIMING UNCERTAINTY MEASUREMENT WITH THE FAST CURRENT PRE-AMPLIFIER - A.R.C. DETECTOR TIMING SYSTEM

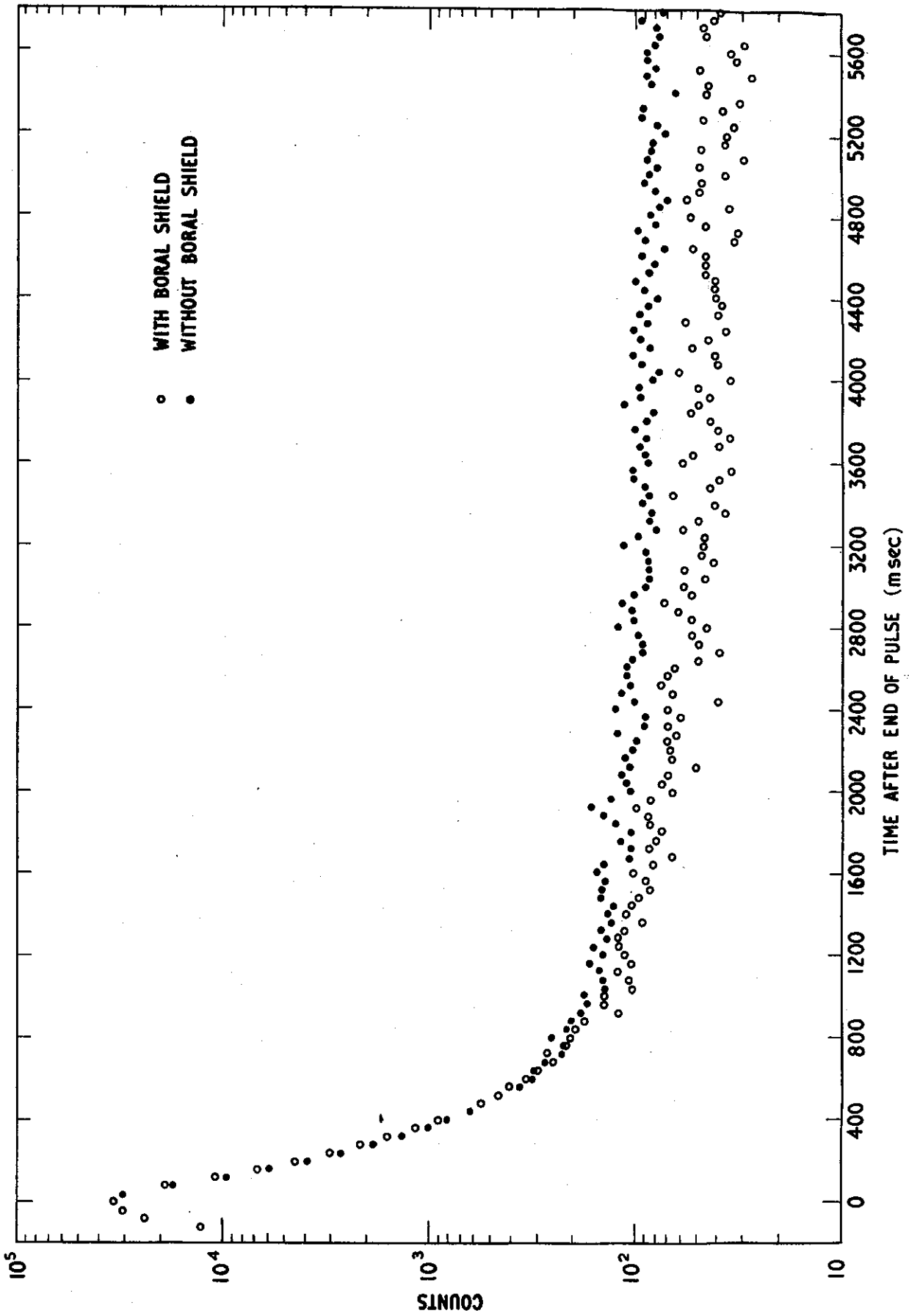


FIGURE 11. EFFECT ON <sup>239</sup>Pu DETECTOR RESPONSE OF A BORAL SHIELD AT THE SURFACE OF THE THORIUM ASSEMBLY

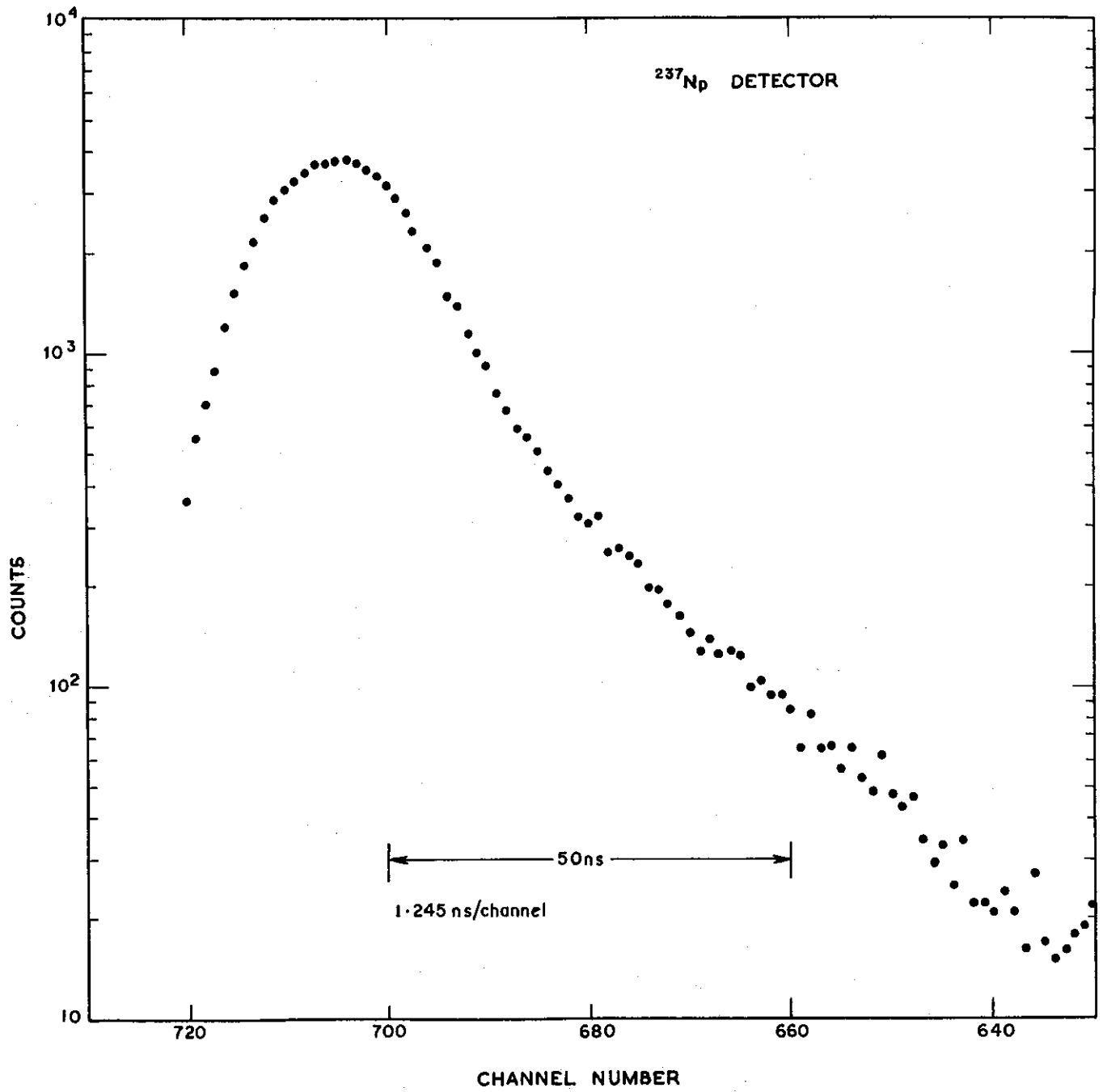


FIGURE 12. TIME DEPENDENT REACTION RATE OF A  $^{237}\text{Np}$  DETECTOR IN THE PULSED THORIUM ASSEMBLY

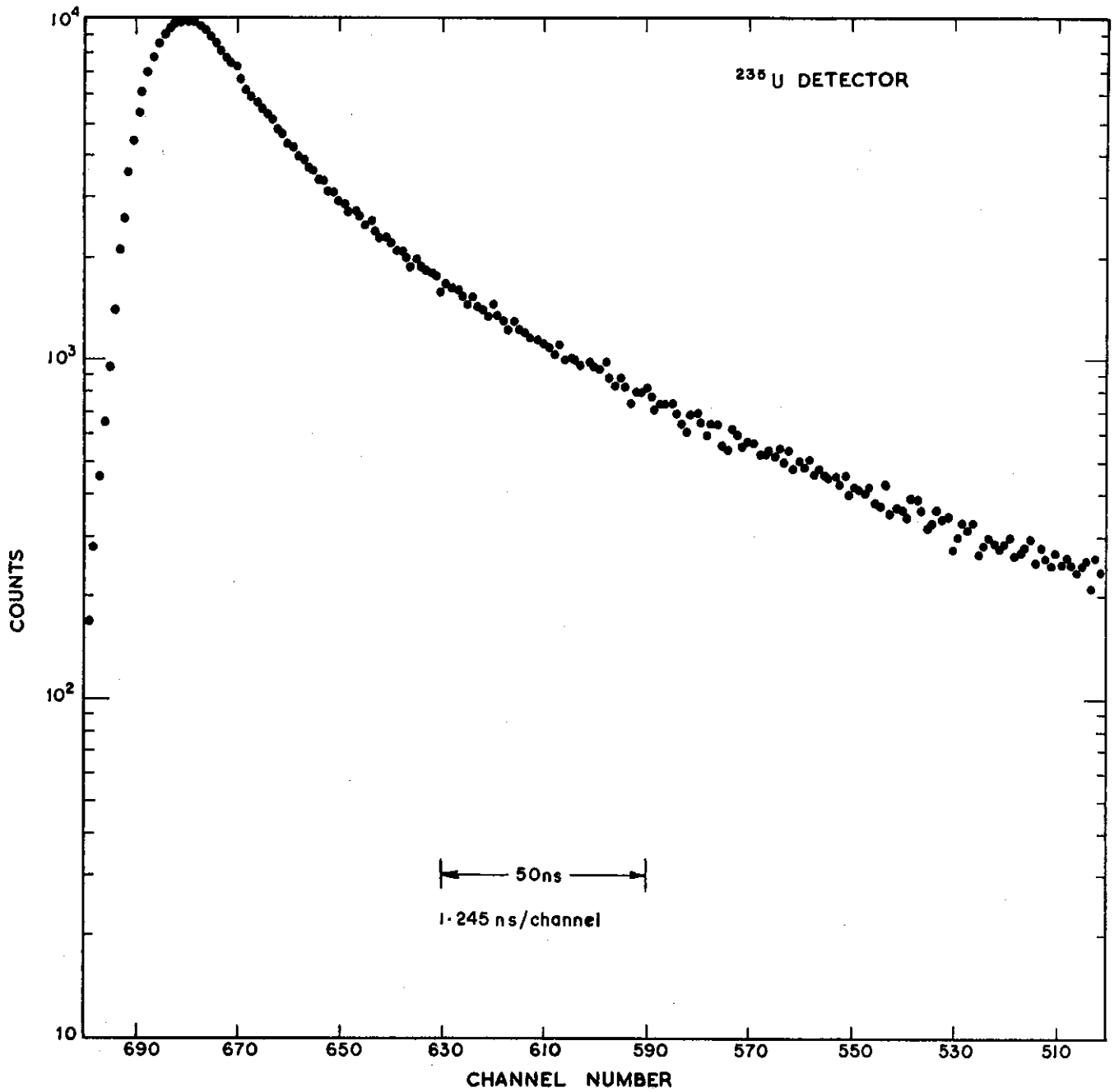


FIGURE 13. TIME DEPENDENT REACTION RATE OF A <sup>235</sup>U DETECTOR IN THE PULSED THORIUM ASSEMBLY

